Tiling Freeform Shapes With Straight Panels: Algorithmic Methods.

Johannes Wallner,[1,2] **Alexander Schiftner,**[2,3] **Martin Kilian,**[2,3] **Simon Flöry,**[2,3] **Mathias Höbinger,**[2,3] **Bailin Deng,**[2] **Qixing Huang,**[4] **Helmut Pottmann** [2,5]

[1] TU Graz [2] TU Wien [3] Evolute [4] Stanford University [5] KAUST

Abstract. *This paper shows design studies with bent panels which are originally rectangular or at least approximately rectangular. Based on recent results obtained in the geometry processing community, we algorithmically approach the questions of an exact rectangular shape of panels; of watertightness of the resulting paneling; and of the panel shapes being achievable by pure bending. We conclude the paper with an analysis of stress and strain in bent and twisted panels.*

1 Introduction

This paper is concerned with panels of wood or metal, which are mounted on freeform surfaces, and which in their flat state are rectangular (or can at least be cut from rectangles). Figure 1 gives an impression of the kind of example we have in mind. In particular we deal with a mathematical formulation and algorithmic approach to this topic. Such patterns occur in the cladding of general freeform (double curved) shapes, for instance applied to interior surfaces. An experimental example, which is taken from [Spuybroek 2004], is shown by Figure 2.

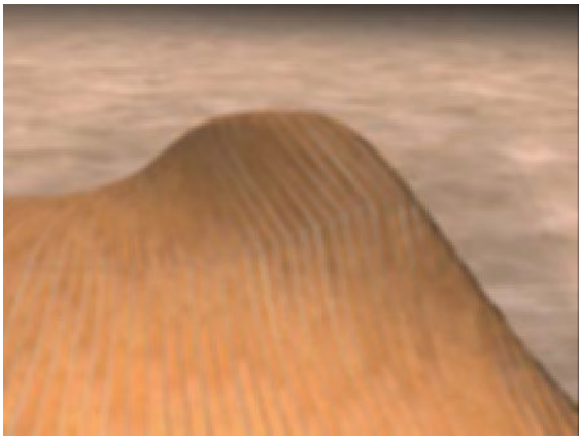

Figure 1: This image gives an impression of rectangular panels mounted on a freeform shape in an optimized pattern: Gaps are deliberately left open in order to illustrate how little the panel widths would have to be modified in order to achieve watertight paneling (cf. Figures 5, 14).

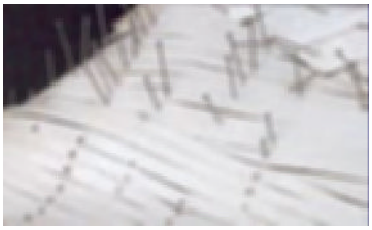

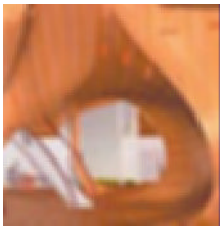

Figure 2: Experimental cladding using paper strips (left) results in an office space design by NOX Architects (right, see [Spuybroek 2004]).

In order to understand the *geometry* which governs the behaviour of panels, we discuss the various issues which arise when trying to cover freeform shapes with rectangular panels. There are several properties of the resulting patterns which one would like to have — each property being derived from practical considerations and giving rise to its own mathematical theory. Unfortunately only in rare instances we can have all of these properties at the same time. Usually a compromise will have to be found.

The geodesic property. Long and thin panels easily bend about their weak axis and may twist a bit, but for all practical purposes they do not bend about their strong axis. This translates into the mathematical statement that such a panel, if laid onto a surface, follows a *geodesic curve*. These curves are equally characterized by having zero geodesic curvature, and by being the shortest curves which connect different points of a surface. For more information on geodesics, the reader is referred to textbooks of differential geometry such as [do Carmo 1976].

The constant width property. We think of panels whose original, unfolded shape is a rectangle (see Figure 2, where those panels are represented as strips of paper). Only special shapes can be covered by such panels in a seamless and non-overlapping way: basically the only way in which this can happen is that the entire surface is itself a *developable surface*. For all other surfaces, assuming we have no gaps or overlaps, panels are not exactly rectangular when unfolded. In any case it is very important for the practical fabrication of such panels that they can be cut from a rectangular shape without too much waste. Mathematically this leads us to the requirement that the geodesic curves which guide the panels must have approximately *constant distance* from their neighbour curves.

The developable (or 'pure bending') property. The process of bending a surface changes the distances of points only by a very small amount, if those distances are measured inside the surface. A certain amount of twisting, as opposed to pure bending, is present in the applications we have in mind. While the previous two properties actively influence all our algorithmic approaches, the developable property is present in only one of them.

The issues discussed above lead to the following questions:

Problem statement 1. *We look for a system of geodesic curves in a freeform surface which are at approximately constant distance from their neighbours, and which can serve as guiding curves for the bending of rectangular wooden panels. Those panels are to cover the surface with only small gaps and no overlaps.*

Problem statement 2. *We look for a system of geodesic curves in a freeform surface which serve as the boundaries of wooden panels whose development is approximately straight and which can be cut from a rectangular shape. Those panels are to cover the surface without gaps.*

Previous work. Questions of this kind and generally the layout of geodesic patterns on surfaces have recently attracted great interest in the geometry processing community. [Kahlert et al. 2010] study the tiling of a surface by strips of controlled width which are bounded by geodesics. They employ an evolution method, starting from a single geodesic and proceeding from there until the surface under consideration is exhausted. [Pottmann et al. 2010] investigate general and multiple patterns of geodesics on freeform surfaces. They propose a mixture of methods (evolution, level set, geodesic vector fields), and it is that paper which our work is mainly based on.

— *Related work: Computing geodesics.* The theory of geodesics is found in textbooks of differential geometry such as [do Carmo 1976]. For computational purposes, shapes are represented as triangle meshes, and their geodesics are represented as polylines in meshes which are the shortest connections between points. That definition is usually sufficient but may lead to ambiguities which can be resolved by the concept of "straightest geodesics" [Polthier and Schmies 1998] which we use in our algorithms. Finding the truly shortest geodesic paths requires the computation of distance fields, for which several efficient algorithms have been developed, see for instance [Chen and Han 1996] or [Kimmel and Sethian 1998], or the later paper [Surazhsky et al. 2005].

— *Related work: Timber constructions and geodesics.* Geodesic curves have made their appearance in freeform architecture in another context, namely in the supporting structures of curved shells. [Pirazzi and Weinand 2006] show the design of freeform timber rib shells which are composed of screw-laminated beams. If such beams are considered as curves in the surface they support, then they have zero geodesic curvature, i.e., they are geodesics.

— *Related work: Rationalization of freeform surfaces by developable strips.* Early research on the cladding of freeform surfaces with developable panels evolved from the architecture of F. Gehry [Shelden 2002]. That work however does not deal with the decomposition of general shapes into developable strips, which problem was algorithmically solved by [Pottmann et al. 2008]. Already in that paper a notion of *geodesic strips* was defined: we discuss them later. The authors emphasize that in general any decomposition of a surface into developable strips must be such that the strip boundaries stay away from the *asymptotic directions* in the saddle-shaped regions of the surface. Differential-geometric issues of that kind will also be present in our work.

2 The Design of Patterns of Geodesics.

As a prerequisite for solving Problems 1 and 2 we first discuss patterns of geodesic curves in surfaces and methods to create them. Subsequent sections translate the geometric information stored in these curve patterns into actual paneling.

Let us rehearse the various properties of geodesics: They are the curves in a surface with zero geodesic (i.e., sideways) curvature. They are uniquely determined by an initial point and tangent. Mathematically, if a point $p(t)$ is moving in time t with unit speed, then it moves along a geodesic if and only if the second derivative vector $p''(t)$ remains orthogonal to the surface. Also the shortest connections between points in the surface are geodesics.

2.1 Design by Parallel Transport.

In this section we describe how to find patterns of geodesics where either the maximum distance or the minimum distance between adjacent curves occurs at a prescribed location. This method is briefly described by [Pottmann et al. 2010].

Differential geometry knows the notion of *parallel transport* of a vector V along a curve s contained in a surface. It means moving that vector along s such that it remains tangent to the surface, but such that it changes as little as possible (i.e., $\|V'(t)\|$ is minimal). It is known that the length of that vector remains unchanged [do Carmo 1976]. If, for computational purposes, a surface is represented as a mesh and a curve is represented as a polyline with vertices $P_0, P_1, P_2, \ldots$, we emulate parallel transport along that polyline by a simple step-by-step procedure explained in Figure 3.

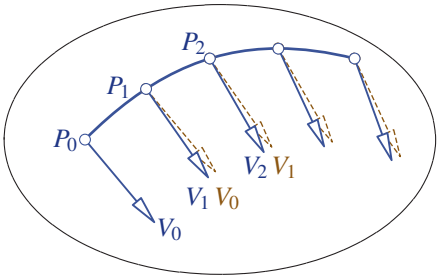

Figure 3: Parallel transport of a vector V_0 attached to the vertex P_0 along the polyline $P_0P_1P_2\ldots$ is algorithmically realized as follows: V_i is found by orthogonal projection of V_{i-1} onto the tangent plane of P_i, and subsequent re-normalizing.

Parallel transport has the following property relevant to the design of patterns of geodesics: Suppose a curve is sampled at points $P_0, P_1, \ldots$ as shown by Figure 3 and that geodesic parallel transport yields vectors $V_0, V_1, \ldots$ attached to these points. Consider the geodesic rays which emanate from the point P_i in direction V_i and $-V_i$ (two such rays together make one unbroken geodesic). Figure 4 shows an example of that. *Then extremal distances between adjacent geodesics occur near the chosen curve*.

Figure 4: Designing a sequence of geodesics by choosing the locus (red) of minimum distance or maximum distance between neighbours. This is done by the *parallel transport method*. In this particular example, the method is applied not to the entire surface, but to previously selected patches.

2.2 Design by Evolution and by Segmentation

We first briefly rehearse the evolution method proposed by [Pottmann et al. 2010]. Starting from a *source geodesic* somewhere in the given surface, we evolve a pattern of geodesics, iteratively computing 'next' geodesics, each having approximately constant distance from its predecessor. This is not possible in an exact way on general surfaces, and if the deviation from a predefined width becomes too great one might to have to introduce breakpoints and proceed further with piecewise-geodesic curves. Figure 5 illustrates how this procedure works; for algorithmic details we refer to [Pottmann et al. 2010].

Another method employed by [Pottmann et al. 2010] is based on the concept of piecewise-geodesic vector fields. We cannot attempt to describe it here, but we mention that it performs *segmentation* of the given freeform shape into parts which are nicely coverable by a pattern of geodesic lines. Both Figure 4 and Figure 6 show an example of this. For Figure 4, the single patches which emerge after segmentation have been treated with the parallel transport method. For Figure 6, the evolution method has been used.

3 Panels from Curve Patterns.

Panels as we consider them are originally flat, and when mounted onto a surface they are bent (and twisted if necessary). We investigate two different ways of mathematical representation of such panels: One which produces almost exactly developable shapes which are achievable by pure bending, and another method where we check for the amount of twisting only afterwards. Unfortunately the first method is hindered by obstructions of a fundamental nature.

The exact relation between the ideal design surface Φ to be covered by the panels on the one hand, and the panels themselves on the other hand, needs clarification. One possibility is that we model the panel surfaces so that they are tangentially circumscribed to Φ along given geodesic curves; and this is what we do.

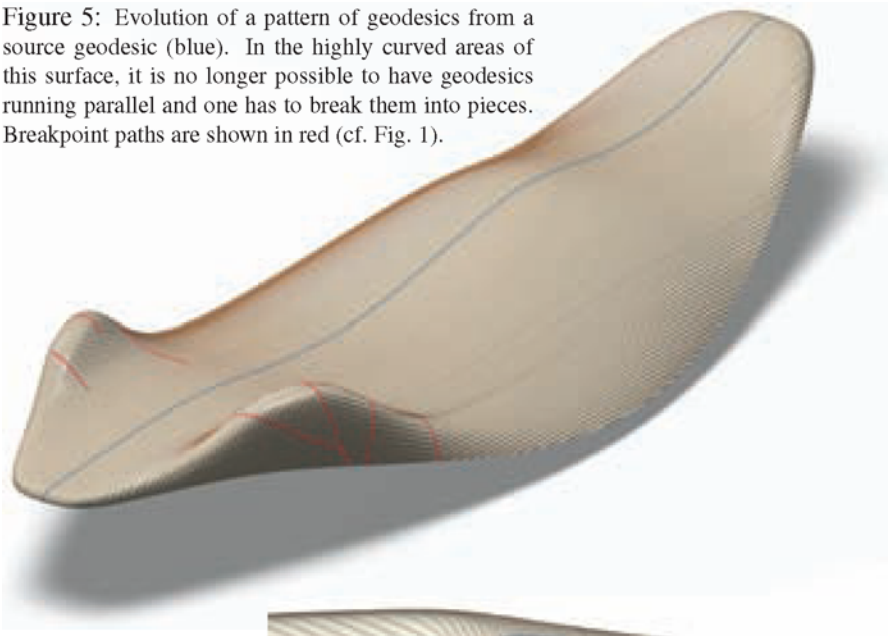

Figure 5: Evolution of a pattern of geodesics from a source geodesic (blue). In the highly curved areas of this surface, it is no longer possible to have geodesics running parallel and one has to break them into pieces. Breakpoint paths are shown in red (cf. Fig. 1).

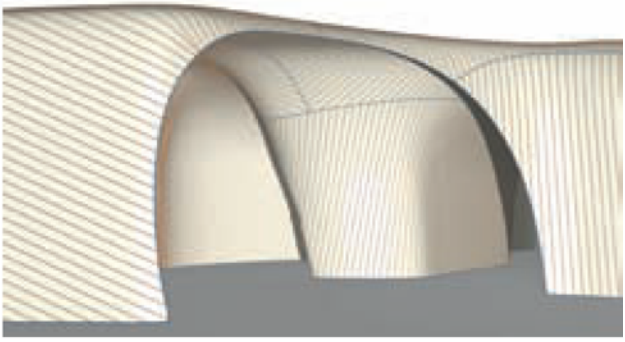

Figure 6: Segmenting a surface into pieces which can nicely be covered by a sequence of geodesic lines. For the covering, the evolution method was employed.

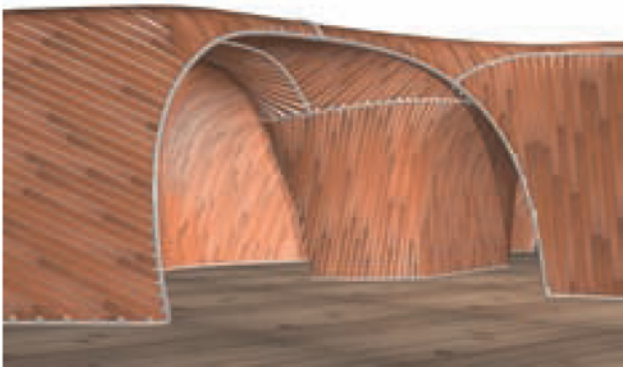

Figure 7: This design with bent rectangular panels is based on Figure 6.

Another idea is that the panel surfaces are *inscribed* into the design surface. For instance we could connect two neighbouring geodesics by a developable surface which is subsequently used for the panel. Algorithmically this is not easy [Rose et al. 2007] and anyway we would rather have a geodesic running in the center of the panel (which is achieved with the idea of circumscribed panels).

3.1 Panels with Pure Bending: the Tangent Developable Method.

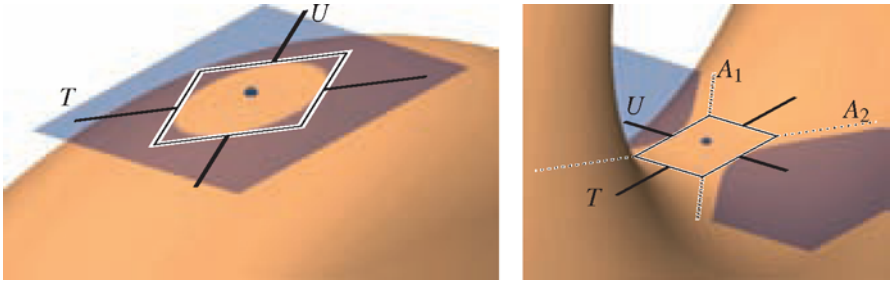

Figure 8: Illustration of asymptotic directions A_1, A_2 and conjugate directions T, U: Parallel translation of a tangent plane (blue) by a small amount and intersection with the surface yields a curve which approximates a conic section (the *Dupin indicatrix*). In negatively curved areas this is a hyperbola, whose asymptotes A_1, A_2 define the *asymptotic directions*. Any parallelogram tangentially circumscribed to the indicatrix defines two conjugate tangents T, U. It is known that A_1, A_2 are diagonals of any such parallelogram. Obviously choosing T determines U. For both figures, the base surface is a torus.

For smooth surfaces the notion of *conjugate tangents* is defined; they are explained by Figure 8. Mathematically vectors v, w which are expressed in a coordinate system whose basis are principal curvature vectors are conjugate, if and only if $v^T \operatorname{diag}(\kappa_1, \kappa_2) w = 0$, where κ_1, κ_2 are the principal curvatures. Algorithmically, curvatures and conjugate tangents can be computed from triangle meshes by well known methods of geometry processing, see e.g. [Cazals and Pouget 2003].

Conjugate tangents play an important role here because they can be used to create a developable surface Ψ which is tangentially circumscribed to a given surface Φ along a curve s (see Figure 9). That *tangent developable* even has the nice property

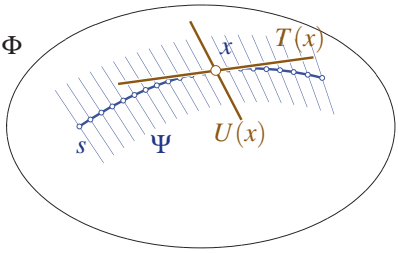

Figure 9: Consider a point x in a geodesic s which lies in the surface Φ. If $T(x)$ is tangent to the geodesic, compute $U(x)$ as being conjugate to $T(x)$. Then the union of all tangents $U(x)$ is a developable ruled surface Ψ which is tangentially circumscribed to Φ along the curve s.

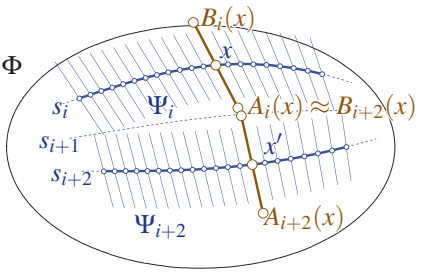

Figure 10: Developable surfaces Ψ_i associated with geodesics with *even* indices i are trimmed by geodesics with odd index.

that s is a geodesic not only for Φ, but also for Ψ. Thus, when Ψ is unfolded into the plane, s becomes a straight line.

This geometric information suggests the following algorithm to create panels: First, for all geodesics s_i in a given geodesic pattern compute the tangent developable Ψ_i according to Figure 9. Trim those surfaces along the intersection curves with their respective neighbours. Unfolding the trimmed Ψ_i's yields the flat state of panels.

Unfortunately this does not work in practice. One reason is that the rulings of the tangent developables may behave in weird ways. Another reason is that the intersection of neighbouring Ψ_s's is often ill-defined, so trimming as suggested will not work. We therefore have chosen the following modified procedure:

1. For the geodesics s_i where i is an even number compute the tangent developable Ψ_i according to Figure 9. That is, for a dense sample of points x on s_i we compute the rulings $U_i(x)$ which are conjugate to the tangent $T_i(x)$.

2. Delete all rulings $U_i(x)$ of Ψ_i where the angle enclosed with the tangent $T_i(x)$ is smaller than some threshold (say, 20 degrees) and fill the holes by interpolation (this is a standard procedure).

3. On each ruling $U_i(x)$ determine points $A_i(x)$ and $B_i(x)$ which are closest to the geodesics s_{i-1} and s_{i+1}, respectively (see Figure 10). This serves for trimming the surface Ψ_i.

4. Optimize globally the positions of points $A_i(x)$ and $B_i(x)$ such that trim curves are smooth, such that $A_i(x)$ and $B_i(x)$ are close to geodesics s_{i-1}, s_{i+1}, and such that the ruling segments $A_i(x)B_i(x)$ lie close to Φ. For this optimization we need the distance fields of Φ and of the single geodesics. We only change the surface a little bit and hope not to lose too much developability.

Figures 11, 12 and 13 illustrate panelizations of freeform shapes obtained by this method. The degree of developability which is achieved can be evaluated by measuring the Gauss curvatures of panel surfaces, such as done by Figure 16. The Gauss curvature vanishes for exact developability. The exact values for the panelizations of Figures 11 and 14, which work with the same design surface and comparable strip width can be seen in the table at the end of Section 4.

Figure 11: Almost-developable strips constituting a watertight surface.

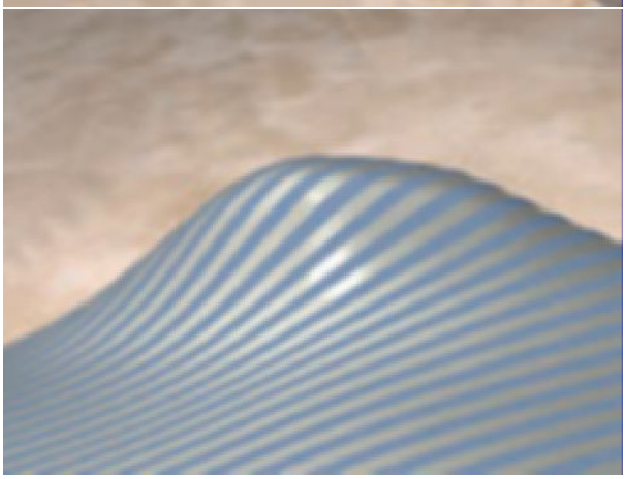

Figure 12: Detail of Figure 11. The gaps in between panels which occur in highly curved areas are hardly visible. The maximal strip width is 0.4% of the entire design's bounding box diagonal.

Figure 13: Watertight panels based on the segmentation and parallel transport methods. See also Figure 4. The intrinsic curvature of the rather broad panels is too high to make this design practicable: its purpose is to illustrate the parallel transport method.

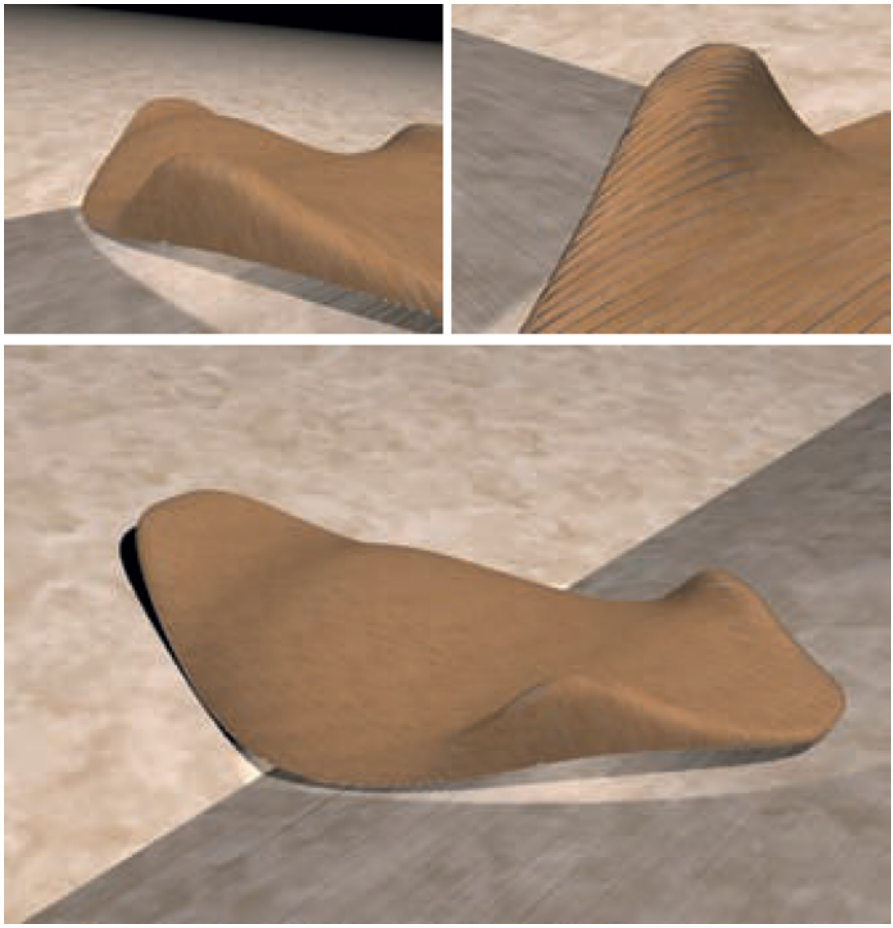

Figure 14: *Below:* A surface is covered by wooden panels of constant width. This is achieved by the 'evolution method' illustrated by Figure 5: The pattern of panels evolves from a well-placed source geodesic as long as the requirement of constant panel width is satisfied up to certain thresholds. If the panel width deviates too much from the desired value, the geodesics are broken. Subsequently panel surfaces have been created by the 'binormal method'. *Above:* Details. A further detail is shown by Figure 1.

3.2 The Binormal Method.

Our second method of defining panels (after a pattern of geodesics in the surface Φ has been found) works directly with the geodesic curves.

Assume that such a geodesic s is traversed by a point $P(t)$ moving with unit speed, where t is a time parameter. For each time t we have the velocity vector $T(t)$, the normal vector $N(t)$ of the surface Φ in the point $P(t)$, and a third vector $B(t)$ (the *binormal vector*) which makes T,N,B a moving orthogonal right-handed frame.

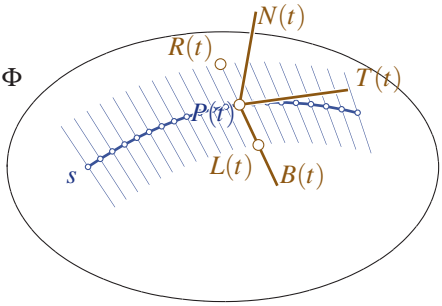

Figure 15: The binormal method defines a ruled panel surface from a central geodesic s via its Frenet frame T,N,B: The ruling passing through the central point $P(t)$ on the geodesic is indicated by the binormal vector $B(t)$. The endpoints of the ruling segment are points $L(t)$ and $R(t)$ whose distance from $P(t)$ is half the intended panel width.

For computational purposes, the surface Φ is represented as a triangle mesh and s is given as a polyline. Numerically the computation of the frame T,N,B is stable if performed in the way described above, despite the fact that it is actually the Frenet frame of s which usually exhibits numerical deficiencies (this connection with the Frenet frame follows from the geodesic property).

For each geodesic, the associated panel surface is constructed according to Figure 15. Panelizations of freeform surfaces which have been achieved with this method are shown by Figures 7 and 14.

3.3 Discussion

The previous two subsections proposed two different methods of defining ideal and mathematically abstract surfaces which are to be followed by panels. The 'tangent developable' method tries to produce panel surfaces which are achievable by pure bending (in fact the tangent developable is the only surface with this property which is also tangent to the original design surface). Thus the mathematical goal of developability is corresponding to a natural manufacturing goal. It seems reasonable to let actual panels exactly follow the surfaces proposed by this algorithmic method.

The situation is slightly different for the second suggested way of defining panel surfaces (the 'binormal' method). From a mathematical viewpoint it is a simple and obvious way of defining panel surfaces, but it is unclear that this surface should be the shape of a panel after it has been forced to follow a geodesic on the surface Φ. Of course such a shape is subject to the existing constraints, but one would assume that panels rather assume shapes achievable by pure bending. The purpose of the binormal method is mainly to pin down a mathematically exact surface, for the practical purpose of having shapes exactly defined. Anyway the following section shows that the panel shapes defined by the binormal method are admissible from the viewpoint of stresses and strain.

4 Stress and Strain in Panels.

This section investigates the deformation a rectangular strip of elastic material experiences when it is bent into the shape of a ruled surface Ψ such that the central line

Figure 16: Visualization of Gaussian curvature of the design shown by Figures 11, 12. Blue corresponds to zero, red to the maximum value -0.02 (this means $\rho = 7.07$). The bounding box diagonal of this object is 188.

m of the strip follows a 'middle geodesic' s in Ψ. This applies to both our methods of defining panel surfaces. It seems a reasonable assumption that the central line is only bent, but not stretched. Due to the saddle shape (negative Gaussian curvature) of all ruled surfaces, the lines parallel to m at distance $d/2$ are not only bent, but also stretched. It is known that after introducing the *radius of Gaussian curvature* $\rho = 1/\sqrt{|K|}$, the relative increment in length (the strain) of the strip boundaries is given by

$$\varepsilon = \frac{1}{2}(d/2\rho)^2 + \cdots,$$

where the dots indicate terms of higher order in d. We are first concerned with tensile stress due to this stretching; for other stresses due to bending and shear see the end of this section. A rough estimate, expressing stress by $\sigma = E\varepsilon$, yields

$$d/2\rho \le C, \quad \text{with} \quad C = \sqrt{2\sigma_{\max}/E},$$

where $\sigma_{\max}$ is the maximum admissible stress and E is Young's modulus. The approximative nature of our computation implies using a suitable safety factor when choosing $\sigma_{\max}$. The value C is a material constant which yields an upper bound $d_{\max} = 2\rho_{\min}C$ for the maximum strip with. With sample values for $\sigma_{\max}$ we get

material	Young modulus E $[N/mm^2]$	maximum stress (sample values) $\sigma_{\max}$ $[N/mm^2]$	constant $C = \sqrt{2\sigma_{\max}/E}$
steel	200000	250	0.05
wood	13000	80	0.11

Strip widths and their admissibility for models shown in this paper are collected in the following table. Since these examples have been selected mainly with a view towards visualization, some are not admissible. However they can easily be made so by choosing narrower panels. The choice of units in this table is arbitrary.

Figure No.	material	actual panel width $[m]$	$\lvert K\rvert_{\max}$ $[m^{-2}]$	$\rho_{\min}$ $[m]$	bounding box size $[m]$	admissible width $[m]$	admissible?
1, 5, 14	wood	$d = 0.7$	0.1	3.16	188	0.7	yes
4, 13	steel	$d \le 0.1$	5	0.44	2.8	0.04	no
	wood					0.1	yes
11, 12	steel	$d \le 0.8$	0.02	7.07	188	0.71	almost

Bending and shear stress. Both bending stress and shear stress for a panel with thin rectangular cross-section depend on the panel thickness h, but not on the panel width d if $h/d \ll 1$; the maximum values of these stresses (denoted by σ, τ in this paragraph) occur on the outer surface of the panel. These values depend on the curvature κ of the panel's central geodesic and the rate of torsion θ of the panel (we have $\sigma = E\kappa h/2$ and $\tau = hG\theta$, where G is the shear modulus). Clearly the panel surfaces obtained by the 'tangent developable' method experience less shear than the ones created by the 'binormal' method. It is a standard matter to combine all stresses (tension, shear, bending) and use this information for checking if the panel's dimensions are admissible.

It is interesting to know how the rate of torsion θ (twist angle per panel length) is related to the Gaussian curvature of the panel: It is known that θ, measured in arc per meter, does not exceed $\sqrt{|K|} = 1/\rho$, where the maximum value occurs in case the central geodesic's tangent happens to be an asymptotic direction of the panel surface [do Carmo 1976].

5 Conclusion.

This paper treats paneling of freeform surfaces with rectangular (or almost-rectangular) panels, which are known to follow geodesic curves. For the layout of a system of geodesics several methods have recently been published. We survey some of them in this paper, especially those which produce geodesics running approximately parallel to each other. We further discuss the panel surfaces themselves under the viewpoint of panel shapes achievable by pure bending and a watertight overall panel surface, and we demonstrate our methods by means of some examples. Finally we discuss tensile and shear stresses in panels which occur when they are mounted on freeform surfaces.

Future research. The connection between geometry and mechanics is a very important and at the same time most challenging issue in any freeform design. One topic of future research therefore is to combine geometric considerations with simple aspects of mechanics – our way of expressing stresses by Gaussian curvature already points in this direction.

Panelization poses many geometric questions whose systematic investigation would be rewarding: For instance, panels in the shape of generalized cylinders which are important for bent glass; and more generally special shapes of panels which are relevant for certain manufacturing techniques and specific applications in building construction. Our aim must generally be to find *construction-aware design tools* which do not generate shapes first and lets us think about manufacturing afterwards, but tools which actively, during the design phase, incorporate the side conditions engendered by manufacturing constraints.

References

CAZALS, F., AND POUGET, M. 2003. Estimating differential quantities using polynomial fitting of osculating jets. In *Symp. Geometry processing*, Eurographics, L. Kobbelt, P. Schröder, and H. Hoppe, Eds., 177–178.

CHEN, J., AND HAN, Y. 1996. Shortest paths on a polyhedron. I. Computing shortest paths. *Int. J. Comput. Geom. Appl. 6*, 127–144.

DO CARMO, M. 1976. *Differential Geometry of Curves and Surfaces*. Prentice-Hall.

KAHLERT, J., OLSON, M., AND ZHANG, H. 2010. Width-bounded geodesic strips for surface tiling. *Vis. Computer*. to appear.

KIMMEL, R., AND SETHIAN, J. A. 1998. Computing geodesic paths on manifolds. *PNAS 95*, 8431–8435.

PIRAZZI, C., AND WEINAND, Y. 2006. Geodesic lines on free-form surfaces: optimized grids for timber rib shells. In *Proc. World Conference on Timber Engineering*. 7pp.

POLTHIER, K., AND SCHMIES, M. 1998. Straightest geodesics on polyhedral surfaces. In *Mathematical Visualization*, Springer, H.-C. Hege and K. Polthier, Eds., 391–409.

POTTMANN, H., SCHIFTNER, A., BO, P., SCHMIEDHOFER, H., WANG, W., BALDASSINI, N., AND WALLNER, J. 2008. Freeform surfaces from single curved panels. *ACM Trans. Graphics 27*, 3, #76, 1–10. Proc. SIGGRAPH.

POTTMANN, H., HUANG, Q., DENG, B., SCHIFTNER, A., KILIAN, M., GUIBAS, L., AND WALLNER, J. 2010. Geodesic patterns. *ACM Trans. Graphics 29*, 4, #43,1–10. Proc. SIGGRAPH.

ROSE, K., SHEFFER, A., WITHER, J., CANI, M., AND THIBERT, B. 2007. Developable surfaces from arbitrary sketched boundaries. In *Symp. Geom. Processing*, A. Belyaev and M. Garland, Eds. 163–172.

SHELDEN, D. 2002. *Digital surface representation and the constructibility of Gehry's architecture*. PhD thesis, M.I.T.

SPUYBROEK, L. 2004. *NOX: Machining Architecture*. Thames & Hudson.

SURAZHSKY, V., SURAZHSKY, T., KIRSANOV, D., GORTLER, S., AND HOPPE, H. 2005. Fast exact and approximate geodesics on meshes. *ACM Trans. Graphics 24*, 3, 553–560. Proc. SIGGRAPH.

Freeform Rigid-Foldable Structure using Bidirectionally Flat-Foldable Planar Quadrilateral Mesh

Tomohiro Tachi

The University of Tokyo

Abstract. *This paper presents a computational design method to obtain collapsible variations of rigid-foldable surfaces, i.e., continuously and finitely transformable polyhedral surfaces, homeomorphic to disks and cylinders. Two novel techniques are proposed to design such surfaces: a technique for obtaining a freeform variation of a rigid-foldable and bidirectionally flat-foldable disk surface, which is a hybrid of generalized Miura-ori and eggbox patterns, and a technique to generalize the geometry of cylindrical surface using bidirectionally flat-foldable planar quadrilateral mesh by introducing additional constraints to keep the topology maintained throughout the continuous transformation. Proposed methods produce freeform variations of rigid-foldable structures that have not been realized thus far. Such a structure forms a one-DOF mechanism with two possible flat states. This enables the designs of deployable structures useful for packaging the boundary of architectural spaces, space structures, and so on.*

1 Introduction

A polyhedral surface composed of rigid facets connected by rotational edges forms a kinetic mechanism: a rigid folding mechanism. Several collapsible structures are proposed using this type of kinetic mechanism, such as Miura-ori [Miura 1980] and eggbox patterns [Brunner 1965] (Figure 1). Such a rigid-foldable and flat-foldable surface is useful as a deployable and transformable structures in an architectural context because of the following advantages.

1. The existence of a collapsed state enables compact packaging of the structure.
2. The synchronized complex folding motion produced by constrained rotational hinges can be controlled with simple manipulation.
3. The transformation mechanism that does not rely on the flexibility of materials can be made out of thick rigid panels and hinges.
4. The watertightness of the surface maintained throughout the transformation is potentially suitable for the envelope of a space, a partition, and the facade of a building.

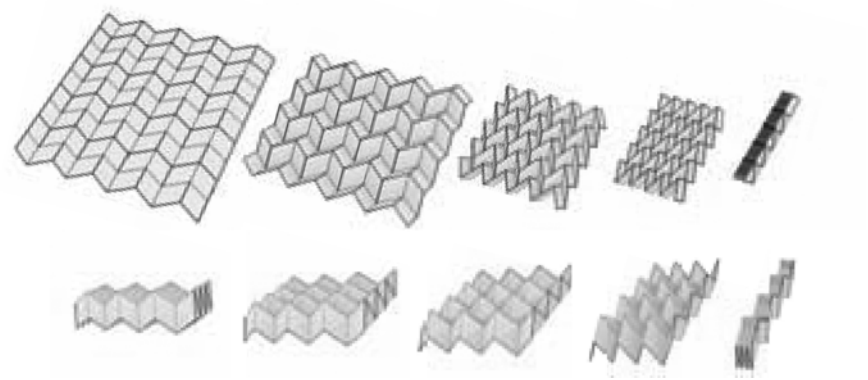

Figure 1: Folding motions of Miura-ori (Top) and eggbox pattern (Bottom).

In order to apply such kinetic surfaces to design purposes, it is required that we can control the three-dimensional shape of the surface and its behavior so that they are consistent with the design requirements. Design requirements in architectural context include environmental conditions, functional requirements, configuration of surrounding buildings and structures, and user's preference. However, since the rigid-foldability of known surfaces strongly relies on the symmetry of the pattern, designing such structures could not be done in an ad-hoc approach; the geometric constraints must be generally investigated to solve an inverse problem of obtaining a pattern from the resulting form and behavior. The objective of our study is thus to freely design kinetic forms using design methods based on computational geometry.

As the first step to achieve this goal, the author proposed a freeform design method of kinetic structures based on origami (developable surface) to provide design variations of Miura-ori through an interactive design system in which a user can deform the surface freely while sustaining the rigid-foldability of the surface ([Tachi 2009a]). This method yields variations of rigid-foldable origami models that have never been achieved otherwise, however, the method was not general enough for design applications, especially of architecture, since the developability condition used is not always an essential condition when we construct structures from multiple parts. In particular, this developability condition disables the design of rigid-foldable collapsible cylinders, realization of which can contribute the designs of surrounding of a volume of a space, collapsible containers, compound surface structures, and so on. This limitation mainly comes from the fact that a cylindrical surface cannot have a globally developed state under the conventional definition.

This paper provides a novel method that enables a freeform variation of such rigid-foldable structure, not restricted by the developability of the surface or the disk topology. We will solve this design problem by extending and combining the ideas of generalized Miura-ori [Tachi 2009a] (or flat-foldable 4-valent-vertex origami)

and generalized eggbox pattern (or discrete Voss surface) [Schief et al. 2007] to produce bidirectionally flat-foldable planar quadrilateral mesh. Such a mesh has nice generalized characteristics: it is bidirectionally flat-foldable and produces one-DOF mechanism. Required design condition is loose compared to purely developable surface and it allows asymmetric and cylindrical variations. We will show a novel design method to obtain rigid-foldable collapsible cylinders by deforming symmetric rigid-foldable cylinders of [Tachi 2009b] into asymmetric ones.

2 Geometry of Rigid-Foldable Quadrilateral Mesh Disk

This section shows the geometry of 4-valency rigid-foldable mesh with two flat states that combines flat-foldable origami surface and discrete Voss surface. A 4-valency mesh or a quadrilateral-mesh surface in general does not enable a continuous rigid-folding motion because an overconstrained system is constructed. This is because the configuration of a rigid-foldable structure homeomorphic to a disk can be represented by the folding angles of edges, while these variables are constrained at each vertex by 3 equations as it is used in the simulation of rigid origami [Tachi 2009c]; if we are to construct a quadrilateral mesh, then the number of constraints exceeds the number of variables only by making 3×3 array. However, Miura-ori [Miura 1980] and eggbox patterns [Brunner 1965] are known to produce singular one-DOF mechanisms (Figure 1) because of their redundant constraints. Miura-ori is a flat-foldable origami surface composed of parallelograms used for packaging of large membranes in the space. The surface produces a synchronized kinetic motion of expanding in x and y directions at the same time from a collapsed state to a completely developed state (Figure 1 Top). Eggbox pattern is a polyhedral surface similarly composed of parallelograms but is not a developable surface. This has two flat-folded states and produces a different one-DOF kinetic behavior from that of Miura-ori; the surface expands in x direction when it collapses in y direction (Figure 1 Bottom). While Miura-ori is a surface with foldlines folded at the same time, eggbox pattern is a surface that has two groups of foldlines collapsed at the same time.

Since Miura-ori and eggbox patterns are surfaces composed of congruent parallelograms, the redundancy of constraints required for the mechanism seem to originate in its global repeating symmetry. However, the condition to produce such redundancy actually is a result of its intrinsic symmetry, i.e., the angles coincidence at each vertex, which also contribute to bi-directional flat-foldability of the surfaces (Miura-ori is developable and flat-foldable. eggbox pattern is flat-foldable in two directions). The intrinsic symmetries of Miura-ori and eggbox pattern, yield generalized forms of rigid-foldable origami surface [Tachi 2009a] and discrete Voss surface [Schief et al. 2007], respectively. In addition, these surfaces can be merged into one generalized hybrid surface, i.e., bidirectionally flat-foldable planar quadrilateral mesh, based on the fact that the behaviors of the two surfaces can be represented using a common form.

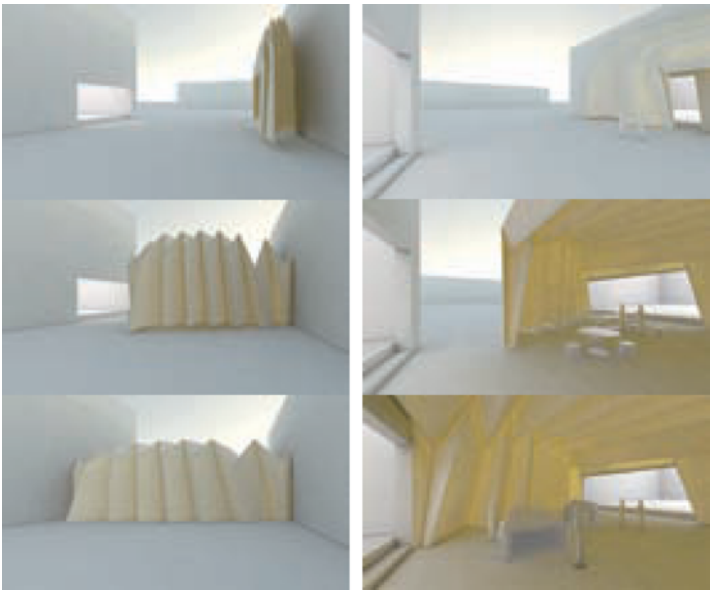

Figure 2: A corrugated vault used as a transformable architecture that connects two existing buildings.

2.1 Generalized Miura-ori

The rigid-foldability condition of generalized Miura-ori is presented by [Tachi 2009a]: consider a planar quad mesh surface of disk topology whose vertices are incident to 4 foldlines; when the surface is developable and flat-foldable, finite rigid-foldability of the surface is equivalent to the existence of one valid semi-folded state. This sufficient condition for rigid-foldability yields rigid-foldable generalization of Miura-ori. The condition also applies to any other degree-4 vertex based patterns such as assymetric vault pattern shown in Figure 2.

The behavior of the surface is represented by the configuration of fold angles. A vertex with 4 foldlines, and thus with 4 sector angles $\theta_i (i = 0,1,2,3)$, form a one-DOF mechanism (Figure 3 Top). In the case of developable and flat-foldable surface, condition of origami (i.e., developability) and flat-foldability given by $\sum_{i=0}^{3} \theta_i = 2\pi$ and $\sum_{i=0}^{3} (-1)^i \theta_i = 0$, respectively, force the sector angles to satisfy

$$\theta_0 = \pi - \theta_2 \quad \text{and} \quad \theta_1 = \pi - \theta_3. \tag{1}$$

According to [Tachi 2009a], the fold angles ρ_i and ρ_j incident to the vertex are related as follows:

$$\tan\frac{\rho_i}{2} = \begin{cases} A_{i,j} \tan\frac{\rho_j}{2} & (i-j = 1 \text{ or } 3 \mod 4) \\ \pm\tan\frac{\rho_j}{2} & (i-j = 2 \mod 4) \end{cases} \tag{2}$$

where the latter represents that pairs of opposite foldlines have an equal absolute folding angles, and $A_{i,j}$ is the coefficient between these two equivalent pairs determined by $\theta_0, \cdots, \theta_3$, i.e., intrinsic measure in the crease pattern independent from the folding angles. Specifically, if $|\rho_0| = |\rho_2| > |\rho_1| = |\rho_3|$,

$$|A_{0,1}| = \sqrt{\frac{1+\cos(\theta_0 - \theta_1)}{1+\cos(\theta_0 + \theta_1)}}.$$

Note that this relationship is a special case of the generalized form of origami vertex presented by [Huffman 1976].

This gives an explicit configuration of folding angles of all foldlines globally connected via degree-4 vertices:

$$\left\{\tan\frac{\rho_i(t)}{2}\right\} = \left\{\tan\frac{\rho_i(t_0)}{2}\right\}\frac{\tan\frac{t}{2}}{\tan\frac{t_0}{2}}, \tag{3}$$

where t $(0 \le t \le \pi)$ is the parameter that defines the folding amount ($t = 0$ and $t = \pi$ indicate developed and flat-folded states respectively) and $\left\{\tan\frac{\rho_i(t_0)}{2}\right\}$ is an arbitrary semi-folded state $(0 < t_0 < \pi)$. Generalized Miura-ori thus shows a kinetic motion of expanding in x and y directions at the same time.

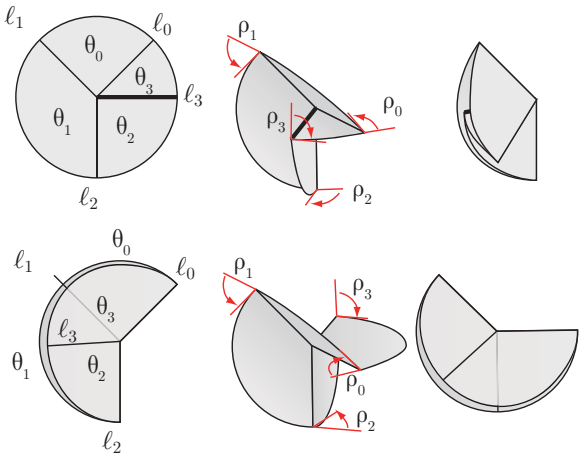

Figure 3: The folding motions of vertices of origami (Top) and discrete Voss surface (Bottom). Note that set of planes used is identical.

2.2 Generalized Eggbox Pattern

Eggbox pattern can be generalized as a discrete Voss surface; the rigid-foldability of discrete Voss surface is proved by [Schief et al. 2007]. Even though the term discrete Voss surface implies a mesh pattern that represents a smooth surface, corrugated surfaces such as eggbox pattern is also included in the family, since it is defined by the intrinsic angular condition that the opposite angles are equal. Every interior

vertex on a discrete Voss surface is incident to 4 edges (or foldlines) and sector angles θ_i ($i = 0,1,2,3$) that satisfy the following:

$$\theta_0 = \theta_2 \quad \text{and} \quad \theta_1 = \theta_3. \tag{4}$$

Note the similarity to (1): in fact, the set of planes that form an origami vertex and eggbox vertex are identical (Figure 3). According to [Schief et al. 2007], the folding angles ρ_i and ρ_j are similarly written as the following form:

$$\tan\frac{\rho_i}{2} = \begin{cases} A_{i,j}\cot\frac{\rho_j}{2} & (i-j = 1 \text{ or } 3 \mod 4) \\ \tan\frac{\rho_j}{2} & (i-j = 2 \mod 4). \end{cases}$$

If we measure the folding angles of one of the opposite pairs by their complementary angles $\rho_i' = \pi - \rho_i$, this becomes

$$\tan\frac{\rho_i}{2} = \begin{cases} A_{i,j}\tan\frac{\rho_j'}{2} & (i-j = 1 \text{ or } 3 \mod 4) \\ \tan\frac{\rho_j}{2} & (i-j = 2 \mod 4). \end{cases} \tag{5}$$

Therefore the kinematics of Miura-ori and discrete Voss surface are essentially identical as represented by Equation (3).

2.3 Hybrid Surface: Bidirectionally Flat-foldable Planar Quadrilateral Mesh

Here, we introduce a new type of functional patterns, i.e., BDFFPQ mesh (defined later), based on combining the geometry of origami and discrete-Voss surface We introduce the concept of *complementary foldlines*, which are edges whose folding angles are measured by their complementary angles, thus a complementary foldline folds from $\pm\pi$ to 0 when an ordinary foldline folds from 0 to $\pm\pi$. By using complementary foldlines (CFLs) along with foldlines (FLs), we can produce a 4-valency network that consistently joins the vertices of origami and discrete Voss surfaces, so that one-DOF kinetic motion exits.

In order to understand this behavior, we define extended "developed state" and "flat-folded state" as follows:

Developed state: A flat state in which every edge has rotational angle of 0 (thus foldlines are unfolded and complementary foldlines are folded).

Flat-folded state: A flat state in which every edge has rotational angle of $\pm\pi$ (the sign shows mountain or valley).

Here, notice that complementary foldlines and foldlines are interchangeable by calling a developed state a flat-folded state and vice versa.

Here we define *bidirectionally flat-foldable planar quadrilateral mesh (BDFFPQ mesh)* a 4-valency network mesh surface that follows the following conditions.

- The surface is polyhedral, i.e., composed of planar facets, and every edge is either FL or CFL.

- The surface has developed and flat-folded states, where the intersection of the overlapped facets is ignored.
- Each interior vertex's incident edges are either 4 FLs, 4 CFLs, or 2 FLs + 2CFLs in which a pair of CFLs or FLs is an opposite pair.

Rigid foldability of such a surface is represented as follows when the surface is homeomorphic to a disk.

Theorem 1 *If and only if BDFFPQ mesh homeomorphic to a disk with more than one interior vertex has one intermediate folded state, the surface is finitely rigid-foldable.*

Proof: Rigid-foldability of a polyhedral disk surface can be represented by the existence of a continuous solution in the configuration space. From the developability and flat-foldability condition, it follows that subnetwork composed of only FLs (CFLs) must divide the surface completely into one or multiple regions each of which is assigned with either $+1$ or -1 such that the signs of adjacent regions are opposite. The sign indicates the orientation of facet in the flat-folded (developed) state. Then the developability and flat-foldability of the network for each vertex is represented as follows:

$$\text{developability:} \quad \begin{cases} \sum_{i=0}^{3} \sigma^{\text{dev}}(i)\theta_i = 0 & \text{for 4CFL or 2FL + 2CFL vertex} \\ \sum_{i=0}^{3} \theta_i = 2\pi & \text{for 4FL vertex,} \end{cases} \tag{6}$$

$$\text{flat-foldability:} \quad \begin{cases} \sum_{i=0}^{3} \sigma^{\text{ff}}(i)\theta_i = 0 & \text{for 4FL or 2FL + 2CFL vertex} \\ \sum_{i=0}^{3} \theta_i = 2\pi & \text{for 4CFL vertex,} \end{cases} \tag{7}$$

where $\sigma^{\text{dev}}(i)$ and $\sigma^{\text{ff}}(i)$ indicate the assigned signs of the facet incident to the sector angle i in the developed and flat-folded states respectively.

A 2FL+2CFL vertex satisfies $\sum_{i=0}^{3} \sigma(i)\theta_i = 0$ for both σ in developed and flat-folded states ($\{\sigma(0),\sigma(1),\sigma(2),\sigma(3)\} = \{1,1,-1,-1\}$ and $\{1,-1,-1,1\}$); therefore $\theta_0 = \theta_2$ and $\theta_1 = \theta_3$. Hence, the vertex is a discrete Voss vertex and the folding motion follows (5). A 4FL or 4 CFL vertex is essentially a vertex of Miura-ori and the folding angles of incident edges follow the kinetic motion represented by (3). Since we represent the folding angles of complementary foldlines by their complementary angles, these relations can be represented in the following single form:

$$\tan\frac{\rho_i}{2} = A'_{i,j} \tan\frac{\rho_j}{2},$$

where $A'_{i,j} = 1/A_{i,j}$ for 4CFL vertices. Since all the foldlines are connected to each other, the transformation follows (3). Therefore if and only if there exists one intermediate configuration $\left\{\tan\frac{\rho_i(t_0)}{2}\right\}$, there exists a continuous valid configurations $\left\{\tan\frac{\rho_i(t)}{2}\right\}$. □

3 Design Variations of Rigid Foldable Surface

For obtaining design variations, we adopt the perturbation based approach used in [Tachi 2009a]. We first obtain a valid existing BDFFPQ mesh in a flat state; this can be done quite easily, e.g., by using a square grid and assigning mountain, valley, complementary mountain, and complementary valley to the edges. Here, we can roughly design the kinetic behavior since an origami vertex tries to expand the surface in two directions at the same time, while a discrete Voss vertex tries to expand in one direction while collapsing in the other direction.

Then we deform the pattern while sustaining the developability and flat-foldability conditions. The configuration of the mesh surface is represented by the coordinates of vertices $\mathbf{x}$ forming a triangular mesh whose edges are either triangulation edges or complementary or ordinary foldlines. This triangular mesh satisfies the planarity condition for each facet and flat-foldability (7) and developability (6) conditions for each interior vertex. Thus an infinitesimal deformation of mesh configuration must satisfy:

$$\mathbf{c}(\mathbf{x}) = \begin{bmatrix} \mathbf{c}^{\mathrm{dev}}(\mathbf{x}) \\ \mathbf{c}^{\mathrm{ff}}(\mathbf{x}) \\ \mathbf{c}^{\mathrm{planar}}(\mathbf{x}) \end{bmatrix} = \mathbf{0}, \tag{8}$$

where $\mathbf{c}^{\mathrm{dev}}(\mathbf{x})$ is a N^{Vint}-vector (N^{Vint} is the number of interior vertices) whose element is

$$\begin{cases} \sum_{i=0}^{3} \sigma^{\mathrm{dev}}(i)\theta_i & \text{for 4CFL or 2FL + 2CFL vertex} \\ 2\pi - \sum_{i=0}^{3} \theta_i & \text{for 4FLvertex,} \end{cases}$$

$\mathbf{c}^{\mathrm{ff}}(\mathbf{x})$ is a N^{Vint}-vector whose element is

$$\begin{cases} \sum_{i=0}^{3} \sigma^{\mathrm{ff}}(i)\theta_i & \text{for 4FL or 2FL + 2CFL vertex} \\ 2\pi - \sum_{i=0}^{3} \theta_i & \text{for 4CFL vertex,} \end{cases}$$

and $\mathbf{c}^{\mathrm{planar}}(\mathbf{x})$ is a vector with dimension of the number of triangulating edges, and its element is its corresponding folding angle ρ_i.

Since the number of variables exceeds the number of constraints for a quadrilateral mesh structure with multiple boundary edges, the Jacobian matrix of the constraint $\left[\frac{\partial \mathbf{c}}{\partial \mathbf{x}}\right]$ is a rectangular matrix whose number of columns exceeds the number of rows. An infinitesimal solution space of this constraint can be calculated as:

$$\Delta\mathbf{x} = \left(\mathbf{I} - \left[\frac{\partial \mathbf{c}}{\partial \mathbf{x}}\right]^{+} \left[\frac{\partial \mathbf{c}}{\partial \mathbf{x}}\right]\right) \Delta\mathbf{x_0}, \tag{9}$$

where $\left[\frac{\partial \mathbf{c}}{\partial \mathbf{x}}\right]^{+}$ is the pseudo-inverse (Moore-Penrose generalized inverse) of the Jacobian matrix, and $\Delta\mathbf{x_0}$ represents an arbitrary vector. Equation (9) calculates the valid perturbation closest to $\Delta\mathbf{x_0}$ by orthogonal projection to the solution space; therefore,

the user input such as the drag motion of vertices through GUI can be used as $\Delta \mathbf{x_0}$ in the implementation system of the method. A larger deformation of the shape can be achieved by accumulating small deformation using Euler integration while eliminating the residual $\mathbf{c}$ by the Newton-Raphson method. Figure 4 shows an example process of design in a design system that can interactively solve Equation 9 while displaying the 3D configuration, flat-folded state, and developed state of the surface. Figure 4 shows an example process of design in a design system that can interactively solve Equation 9 while displaying the 3D configuration, flat-folded state, and developed state of the surface.

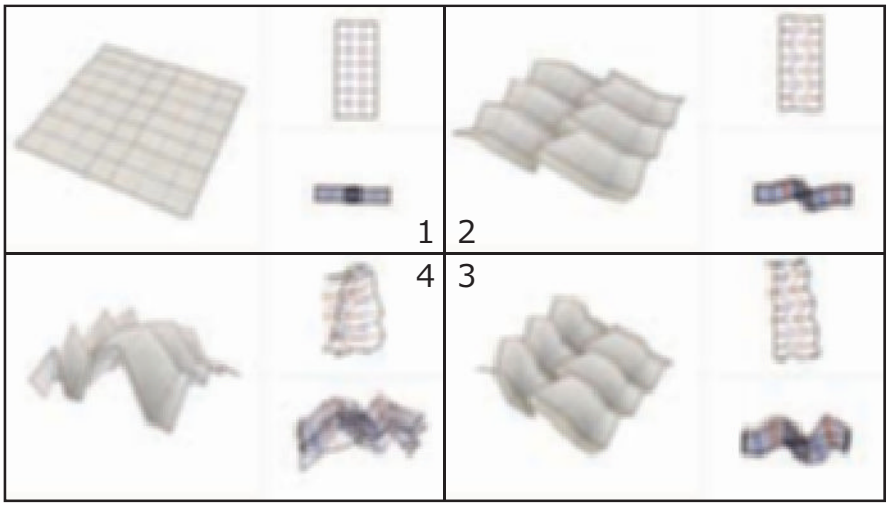

Figure 4: The design process of hybrid pattern obtained by deforming a square grid. Red and dark blue lines indicate mountain and valley foldlines, and pink and light blue indicate complementary mountain and valley foldlines. Each screen shows 3D configuration (left) developed state (upper-right) and flat-foldable shape (lower-right).

The proposed method succeeded in generalizing eggbox pattern and hybrid BDFFPQ mesh. Figure 5 shows an example of a generalized eggbox pattern that has "globally" positive curvature surface, and Figure 6 is an example complex foldable structure based on hybrid surfaces.

4 Rigid Foldable Cylinder

In an architectural context, collapsible cylindrical surfaces are a significant design target since a cylinder qualitatively surrounds a volume of space. Here, note that a cylindrical surface is one of the best possible solutions in this direction since a

Figure 5: The folding motion of a generalized eggbox pattern.

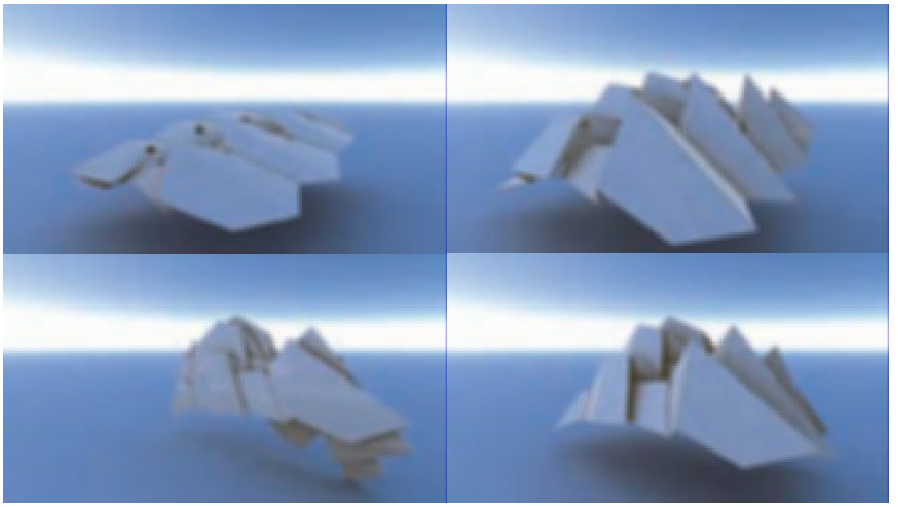

Figure 6: The folding motion of hybrid BDFFPQ mesh.

topologically closed polyhedron, which is ideal in the sense of enclosure of a space, is actually known to forbid a rigid folding motion with volume change as the bellows conjecture [Connelly et al. 1997] states. Although several designs are proposed to enable collapsible and non-rigid-foldable cylinders such as triangulated cylinders [Guest and Pellegrino 1994] and single curved corrugated surface [Hoberman 1993], these exiting designs relied on the flexibility of each facet for the folding motion; they were not applicable to smooth kinetic mechanisms that work with stiff materials and mechanical hinges often required for architectural-scale structures.

[Tachi 2009b] gives a family of cylindrical surfaces and compounds of cylinders that are rigid-foldable and flat-foldable, by solving the angular identity equations via constructing a symmetric modular cylinder based on rotational symmetry and then array copying the obtained module in an axial direction. This successfully produces

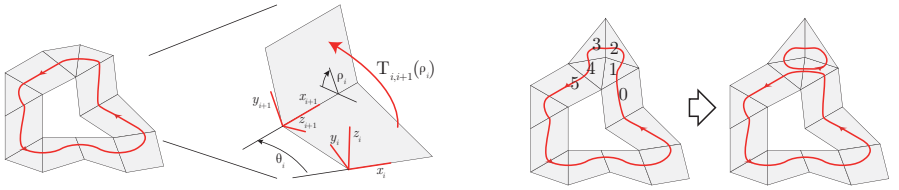

Figure 7: A closed strip of facets (Left). A loop can continuously shrink or expand using conditions around vertices (Right).

a folding motion that does not separate the structure into an open disk. However, the derived surface can only have a constant section along an axis in this approach, and the design variations are limited. Producing freely designed cylindrical surface is the goal of the work described in this section.

The biggest issue in the design of cylindrical surface is that the local condition around each interior vertex is not enough because loops surrounding a hole can geometrically separate by folding; and therefore cylindrical BDFFPQ mesh is not proved to be rigid-foldable in general. In general, it is required that for any closed strip consisting of k facets, the strip does not separate by the folding motion of hinges. We assign a local coordinate to each facet i and denote the local affine transformation from i-th to $i+1$-th coordinates by 4×4 matrix $\mathbf{T}_{i,i+1}(\{\rho_i\})$ (Figure 7 Left). This transformation is regular and the inverse can be described as $\mathbf{T}_{i,j}^{-1} = \mathbf{T}_{j,i}$. The condition thus is represented as, *there exists a vector function* $\rho_i(t)$ $(0 \leq t \leq \pi)$ *that satisfies the following for any loop of facet strip:*

$$\mathbf{T}_{0,1}\mathbf{T}_{1,2}\cdots\mathbf{T}_{i,i+1}\cdots\mathbf{T}_{k,0} \equiv \mathbf{I}. \tag{10}$$

If the facet fan around each vertex is ensured to be rigid-foldable, loop condition around the vertex modifies the condition along a loop to another homologous loop. For example, in Figure 7 right, the transformation from facet 0 to 5 can be simplified as:

$$\mathbf{T}_{0,1}\mathbf{T}_{1,2}\mathbf{T}_{2,3}\mathbf{T}_{3,4}\mathbf{T}_{4,5} \equiv \mathbf{T}_{0,1}\mathbf{T}_{1,4}\mathbf{T}_{4,5}, \tag{11}$$

using the condition around an interior vertex: $\mathbf{T}_{1,2}\mathbf{T}_{2,3}\mathbf{T}_{3,4}\mathbf{T}_{4,1} \equiv \mathbf{I}$. Therefore, the rigid-foldability of a disk with a hole (or n holes) can be represented by the combination of the local rigid-foldability around each interior vertex and the condition around the hole (or the n-holes).

Since BDFFPQ mesh satisfies local rigid-foldability conditions around vertices, the problem of obtaining a rigid-foldable cylindrical BDFFPQ mesh turns into a problem of obtaining a state with one rigid-foldable loop connected to the surface. We transform an existing rigid-foldable cylinder while ensuring the rigid-foldability of one loop satisfied. In order to do this, we use an isotropic type of rigid-foldable cylinders from [Tachi 2009b] as an initial state, which are symmetrically repeating structures constructed using the combination of degree-4 vertices termed *folds* and

elbows producing a valid loop motion, where a fold and an elbow are symmetric cases of origami vertex and discrete Voss vertex, respectively, in our interpretation. Therefore the cylinder is a symmetric type of rigid-foldable cylindrical BDFFPQ.

Since the exact rigid-foldability condition around a loop is still not fully investigated, we guarantee the rigid-foldability of the whole model by using a sufficient condition: one loop around the hole is unchanged from the original symmetric cylinder. We pick up a strip loop along one of the boundaries that exactly produces a one-DOF motion and rigidify this part using a rigid bar model, while we deform other parts under the local conditions of developability, flat-foldability, and planarity of polygons. The developability and flat-foldability keep the sector angles incident to vertices between rigid strip and flexible BDFFPQ strips fixed and enable a one-DOF motion.

We obtained asymmetric form variations from one symmetric cylindrical structure using the design system that solves BDFFPQ mesh and extra constraints. The design process is shown in Figure 8, and Figure 9 shows the derived crease pattern of the design. The pattern shows the location of foldlines in the developed state (note that the lines are drawn on multiple layers since we use extended definition of developed state). Here, we can notice sets of parallel lines remaining in the generalized pattern. This implies the limitation of our method since this globally symmetric behavior forbids cylinders to change their overall radius; this may restrict the design applications of the cylinders. Since this behavior presumably originates in the fixed boundary of the surface, investigating the exact rigid-foldability condition around a loop and loosening the design constraints can contribute to more flexible designs of rigid-foldable cylinders, which still remains to be a future work.

5 Materialization

Because of the developability of the surface, the structure applied for a small scale object can be manufactured from sheets of material such as paper and plastics. The pattern can be first perforated by cutting plotter, laser cutter, or other CNC 2-axis machines on sheets of thin and hard materials, then pasted together, and folded to form a three-dimensional shape. Careful folding control is needed only at the beginning of the fold; once it is semi-folded, the surface folds automatically since the pattern produces a one-DOF motion. Figure 10 shows a folded model of a rigid-foldable cylinder designed using the proposed method.

For a larger scale architectural structure such as shades, retractable roofs, and transformable partitions, the following thickening method can be used to produce a robust kinetic structure. Each facet is first substituted by two layers of constant thickness panels whose contact plane is the ideal geometric surface. In order to avoid the intersection of panels by the folding motion of $0 \leq \rho_i \leq \pi - \delta_i$ for each foldline, the boundary of the panel in the valley side of the surface is relocated on an offset of the foldline by $t \cot \frac{\delta}{2}$, where t is the thickness of the panel (Figure 11). This yields

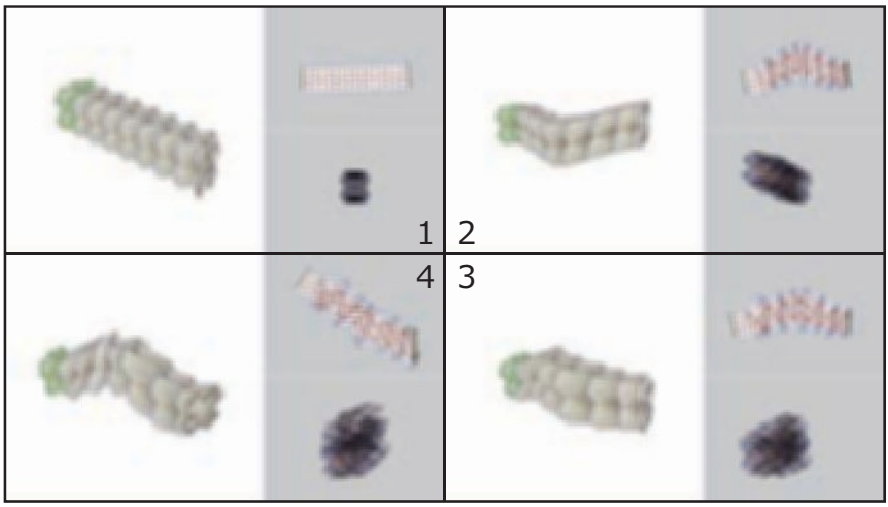

Figure 8: A design process of rigid-foldable cylinder. The initial state is a cylinder by [Tachi 2009b]. The surface is deformed keeping the condition of BDFFPQ mesh while a loop strip (two strips in this redundant case) is maintained to be rigid, as indicated by green rigid bars.

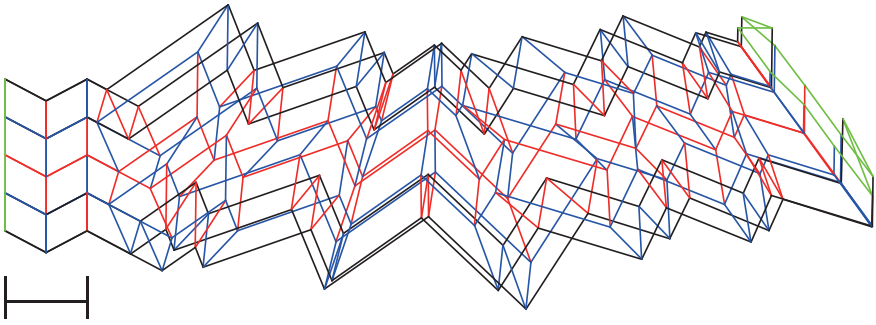

Rigid Part

Figure 9: A crease pattern of generalized cylinder.

designs of kinetic structure composed of rigid panels using their edges as rotational hinges as shown in Figures 12 and 13. The hinges can be constructed mechanically or using a sheet or cloth of negligible thickness between panels; in the latter method, the cloth also becomes a watertight covering.

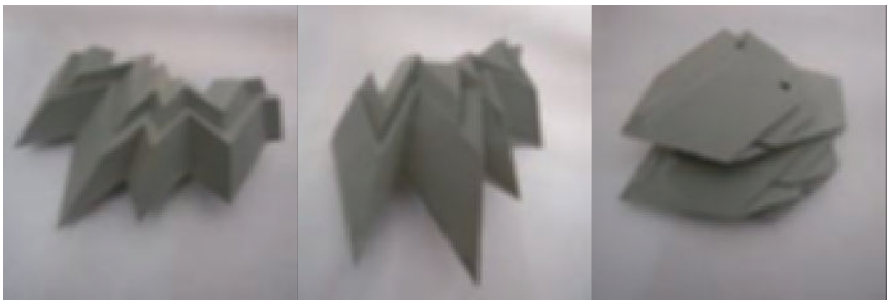

Figure 10: Folded model of a rigid-foldable cylinder. Left: in the developed state, Middle:Intermediate state, Right: flat-folded state.

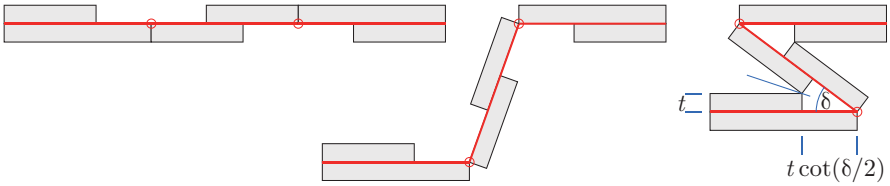

Figure 11: Thickening using two layers of constant thickness panels.

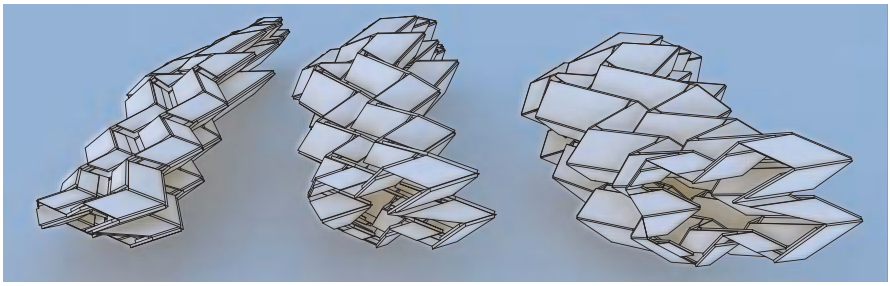

Figure 12: Cylindrical rigid-foldable BDFFPQ mesh consisting of thick panels.

6 Conclusion

In this paper, we presented a design method of rigid-foldable flat-foldable disks and cylinders by introducing bidirectionally flat-foldable planar quadrilateral (BDFFPQ) meshes and their generalization method. The concepts of BDFFPQ mesh, complementary foldlines, and extended definitions of developed and flat-folded states successfully unify and generalize the flat-foldable origami and discrete Voss surfaces. This generalization enables the perturbation based method that can

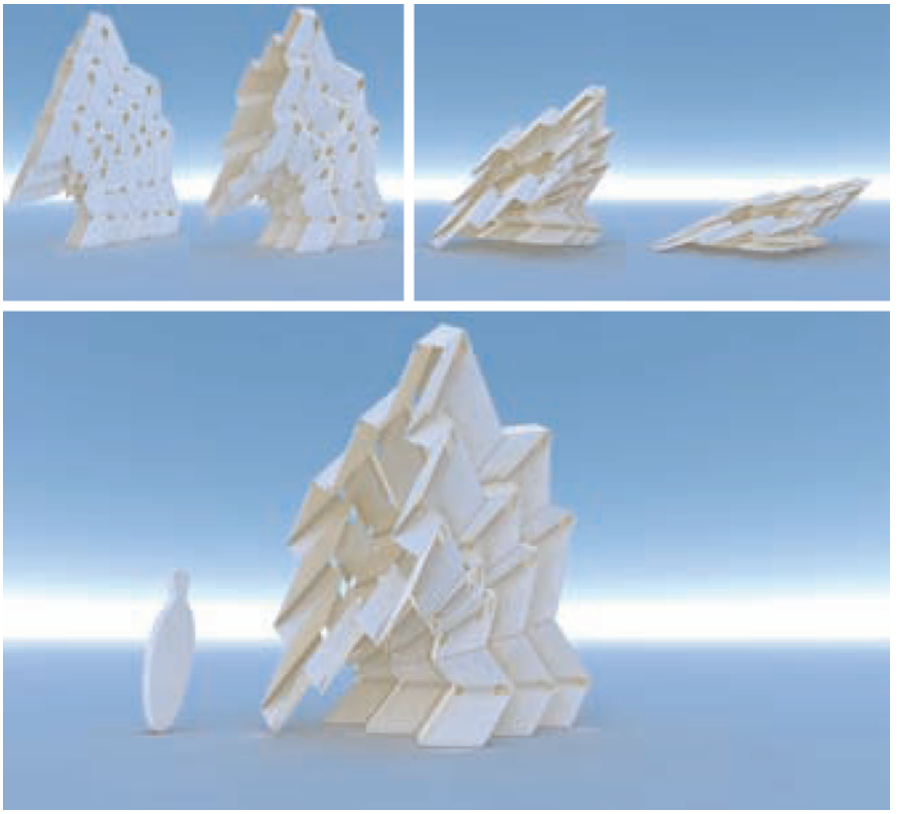

Figure 13: Folding motion of cylindrical structure using thick panels.

freely control the shape of the surface in a direct way; the method yields various designs of rigid-foldable and bidirectionally flat-foldable polyhedral disk. We also investigated the rigid-foldability of a cylindrical surface and its sufficient condition to design a rigid-foldable cylinder. A design method by modifying a cylindrical BDFFPQ mesh with one fixed loop copied from a known rigid-foldable cylindrical structure is introduced. The method enables us to obtain a novel generalized form of rigid-foldable flat-foldable surfaces that can be implemented for architectural design purposes.

It should be noted that we used sufficient condition of the rigid-foldability in this paper and did not provide the exact condition, which still remains to be an unsolved problem as it is seen in [Stachel 2010]. The sufficient condition for enabling cylindrical topology also made the deformation less flexible, the effect of which can be observed in the globally parallel edges. Deriving a more general condition of the rigid-foldability of cylindrical surface and thus enabling a less constrained design is one of the future works of this study.

References

BRUNNER, A., 1965. Expansible surface structure. United States Patent 3,362,118.

CONNELLY, R., SABITOV, I., AND WALZ, A. 1997. The bellows conjecture. *Contributions to Algebra and Geometry 38*, 1, 1–10.

GUEST, S. D., AND PELLEGRINO, S. 1994. The folding of triangulated cylinders, Part I: Geometric considerations. *ASME Journal of Applied Mechanics 61*, 773–777.

HOBERMAN, C., 1993. Curved pleated sheet structures. United States Patent No. 5,234,727.

HUFFMAN, D. 1976. Curvature and creases: a primer on paper. *IEEE Transactions on Computers C-25*, 10, 1010–1019.

MIURA, K. 1980. Method of packaging and deployment of large membranes in space. In *31st Congress of the Internatinal Astronautical Federation*.

SCHIEF, W. K., BOBENKO, A. I., AND HOFFMANN, T. 2007. On the integrability of infinitesimal and finite deformations of polyhedral surfaces. In *Discrete Differntial Geometry (Oberwolfach Proceedings)*, 67–93.

STACHEL, H. 2010. A kinetic approach to Kokotsakis meshes. *Computer Aided Geometric Design*, 27, 428–237.

TACHI, T. 2009. Generalization of rigid-foldable quadrilateral-mesh origami. *Journal of the International Association for Shell and Spatial Structures 50*, 3 (December), 173–179.

TACHI, T. 2009. One-DOF cylindrical deployable structures with rigid quadrilateral panels. In *Proceedings of the IASS Symposium 2009*, 2295–2306.

TACHI, T. 2009. Simulation of rigid origami. In *Origami*^{4}*: The Fourth International Conference on Origami in Science, Mathematics, and Education*, A K Peters, R. Lang, Ed., 175–187.